

Capacitor Condition Monitoring for Modular Multilevel Converter Based on Charging Transient Voltage Analysis

Hongjian Xia^{ID}, Student Member, IEEE, Yi Zhang^{ID}, Member, IEEE, Minyou Chen^{ID}, Senior Member, IEEE, Wei Lai^{ID}, Member, IEEE, Dan Luo^{ID}, and Huai Wang^{ID}, Senior Member, IEEE

Abstract—This article proposes a capacitor condition monitoring (CM) method for modular multilevel converter (MMC) in motor drive applications. The proposed method is based on wavelet decomposition of transient voltage signals, which is independent of modulation schemes and control strategies. The equivalent series resistance (ESR) change can be detected with a moderate computation requirement. Both simulation and experimental results have verified the performance of the proposed method.

Index Terms—Capacitor, condition monitoring (CM), modular multilevel converter (MMC), transient voltage analysis, wavelet.

I. INTRODUCTION

MODULAR multilevel converters (MMCs) are becoming popular in medium-voltage variable-speed motor drives due to its superior performance in modularity and scalability, etc. [1]. The difference of it compared to that of conventional high voltage direct current (HVdc) applications are mainly in two aspects: 1) the aluminum electrolytic capacitors (Al-caps) are usually adopted for its higher power density and low cost [2]; 2) the MMC in motor drives often integrate multiple control strategies or modulation schemes to adapt to varied operation conditions [3], [4], [5].

Condition monitoring (CM) for Al-caps in MMC is essential for system prognostics and health management [6], the proposed CM methods in previous studies are summarized in Table I. First, many methods are mainly developed for HVdc-based applications [7], [8], [9], [10], [11], [12]. The circulating current in the MMC generates capacitor voltage ripples, which are feasible to estimate the capacitor health status. For instance, Ronanki and Willianson [7] utilized the inherent circulating current to estimate the capacitance, while the authors in [8], [9],

and [13] inject additional high-frequency circulating current to enhance the health-relevant signals. Meanwhile, some literature derive the capacitor health status based on specific modulation schemes, such as the estimation of the capacitance based on the phase-shifted carrier (PSC) [10], [14], and the nearest level modulation (NLM) [11], [12]. Therefore, the aforementioned CM methods based on specific modulation schemes and control strategies have limited applicability for the motor drives applications.

The CM methods in the state of the art that have better applicability to different modulation schemes and control strategies are also summarized in Table I [15], [16], [17], [18], [19], [20], [21]. Some of these methods utilize additional hardware to measure the capacitor health-relevant information, such as the reference submodule (SM) in [17] and [18], the tunnel magnetoresistance sensor in [19]. However, the introduced hardware in both methods require additional sensors and signal conditioning circuits, the excessive cost might be questionable for drive applications. The other kind of these methods use multiple software-only-based algorithms to estimate the capacitance, such as the recursive weight least square [15], [22], Kalman algorithm [16], etc. However, the complex algorithms are often prohibitively resource-consuming. Therefore, the motor drive-based MMC needs a cost-effective CM method that is flexible to different modulation schemes and control strategies with moderate implementation complexity.

Compared to the steady-state information used in the aforementioned literature, the transient information is less affected by the control strategies or modulation schemes. The authors in [23] and [24] pointed out that the capacitor charging transient voltage is able to reflect the equivalent series resistance (ESR), which is one of the capacitor health indicators. Specifically, Zhao et al. [23] estimated the capacitor parameters in a buck converter by utilizing the transient information. Furthermore, a wavelet-based CM method is proposed for a boost converter [24], which demonstrates the feasibility to estimate the capacitor ESR via charging transient. However, the above methods are challenging to be extended to the MMC directly. First, the additional hardware cost in [23] and [24] is proportional to the number of capacitors in the converter, which is acceptable in buck or boost converter, however, excessive in the MMC. Second, the computational requirement of the wavelet transform is relevant to the chosen wavelet's complexity. Accordingly, the dedicated

Manuscript received 28 April 2022; revised 19 September 2022; accepted 28 October 2022. Date of publication 3 November 2022; date of current version 26 December 2022. Recommended for publication by Associate Editor D. Dujic. (Corresponding author: Yi Zhang.)

Hongjian Xia, Minyou Chen, Wei Lai, and Dan Luo are with the State Key Laboratory of Power Transmission Equipment & System Security and New Technology, Chongqing University, Chongqing 400044, China (e-mail: hongjian_xia@cqu.edu.cn; mchencqu@126.com; laiwei@cqu.edu.com; walluodan@163.com).

Yi Zhang and Huai Wang are with the AAU Energy, Aalborg University, 9220 Aalborg, Denmark (e-mail: yiz@energy.aau.dk; hwa@et.aau.dk).

Color versions of one or more figures in this article are available at <https://doi.org/10.1109/TPEL.2022.3219291>.

Digital Object Identifier 10.1109/TPEL.2022.3219291

TABLE I
COMPARISON WITH THE EXISTING CAPACITOR CM METHODS FOR MMC

Refs	Method	Software	Additional hardware		Applicable for control
			Sensors	Signal conditioning	
[7]	Second-harmonic impedance	++	N	N	N
[8], [9], [13]	High frequency source injection	+	unknown	Y	N
[10]	Fundamental frequency response in PSC	++	N	N	N
[11]	Capacitor voltage variation in NLM	++	N	N	N
[12]	Submodule switching times in NLM	+	N	N	N
[14]	Capacitor voltage phase in PSC	++	N	N	N
[15]	Recursive weight least square method	+++	N	N	Y
[16]	Kalman filter	+++	N	N	Y
[17], [18]	Reference submodule	+	Y	Y	Y
[19]	Tunnel Magnetoresistance sensor	+++	Y	Y	Y
[20]	Adaptive observer	+++	N	N	Y
[21]	Fast-affine projection algorithm	+++	N	N	Y
Proposed method	Charging transient voltage analysis	+	N	Y	Y

“ Y ” means Yes, and “ N ” means No.

first-order derivative of Gaussian function in [24] would bring heavy computations in MMC. Therefore, further study to extend the charging transient voltage-based method is still necessary.

This article proposes a capacitor CM method for the MMC based on the charging transient voltage analysis. The contributions lie in three folds as follows.

- 1) The relationship between the ESR and the capacitor charging transient voltage is established, and a CM method which is not limited to specific modulation schemes and control strategies is then proposed based on it.
- 2) Combined with a band pass filter, the Haar wavelet-based discrete wavelet transform (DWT) is selected to extract the voltage step from the capacitor voltage [25]. As shown in Table I, the proposed method in this article reduces the hardware complexity by only employing signal conditioning circuits. Meanwhile, the software computational cost is also reduced with the selected Haar wavelet.
- 3) The further implementation methods have been investigated comprehensively, including the sampling frequency presetting, the potential error, and the effect of noise.

The outline of this article is summarized as follows. Section II analyses the relationship between ESR and voltage step at the moment of capacitor charging. Section III proposes the wavelet-based CM method to estimate the ESR with the transient voltage step. Section IV presents the hardware design and analyzes the estimation error considering practical implementation. Sections V and VI verify the proposed method in the simulation and experiments, respectively. Finally, Section VII concludes this article.

II. CAPACITOR CHARGING TRANSIENT VOLTAGE IN MMC

This section analyzes the relationship between the capacitor charging transient voltage and the ESR. The ESR change serves as an indicator of the capacitor health status.

A. MMC Configuration

The topology of a typical three-phase MMC system is shown in Fig. 1. The MMC consists of six arms. Each arm has N SMs

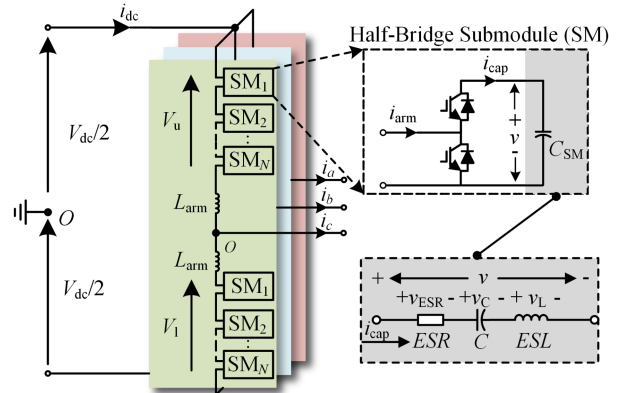


Fig. 1. Circuit configuration of a typical three-phase MMC.

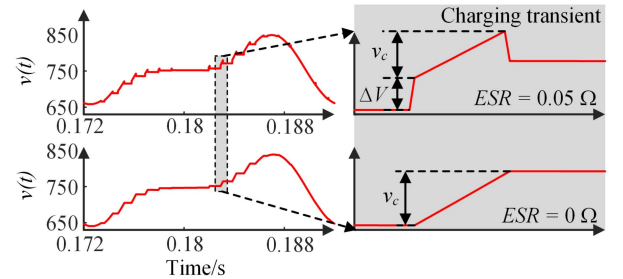


Fig. 2. Simulated ESR's effect on the capacitor's terminal voltage (simulation parameters: rated power $P = 1.2$ MW, $V_{dc} = 8000$ V, and $N = 10$).

and an arm inductor L_{arm} . V_u and V_l are the upper and lower arm voltages, respectively, and V_{dc} is the dc voltage. The SM consists of two insulated gate bipolar transistors (IGBTs) and a capacitor bank (C_{SM}). i_{arm} and i_{cap} are the arm and the capacitor charging current. The capacitor terminal voltage is denoted as v .

B. ESR Effect on the Capacitor Charging Transient

To illustrate the effect of the ESR on the capacitor's charging transient voltage, a simulated case study is shown in Fig. 2. The

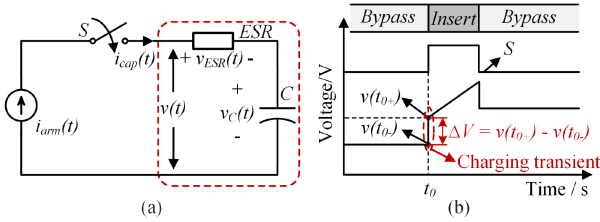


Fig. 3. Capacitor charging transient analysis. (a) Simplified circuit. (b) Capacitor terminal voltage during the charging transient.

ideal capacitor with $ESR = 0 \Omega$ has a smoothly charging process, whereas the capacitor with $ESR = 0.05 \Omega$ has a voltage step at the charging moment. It implies that the capacitor's charging transient behavior is possible to be used to monitor the ESR.

To establish the analytical relation between the ESR and the voltage step, the capacitor's charging transient is equivalent, as shown in Fig. 3(a), and the capacitor terminal voltage is expressed as

$$v(t) = v_C(t) + v_{ESR}(t) \quad (1)$$

where v_C is the voltage across the pure capacitor, and v_{ESR} is the voltage drop of the ESR. Since the switching frequency in the MMC is mainly less than the order of kHz, the equivalent series inductance (ESL) is ignored in the following analysis.

The charging transient process is illustrated in Fig. 3(b). When the SM is inserted ($S = 1$), the capacitor is charged or discharged depending on the direction of the arm current. When the SM is bypassed ($S = 0$), the capacitor maintains its voltage. Assuming the SM is inserted at t_0 and the arm current is positive, then the instantaneous charging current $i_{cap}(t)$ at t_0 is expressed as

$$i_{cap}(t_0) = i_{arm}(t_0) \cdot H(t_0) \quad (2)$$

where $H(t_0)$ is the unit step function at t_0 .

According to (1) and (2), the capacitor voltage at t_0 is expressed as

$$v(t_0) = v_C(t_0) + \Delta V \cdot H(t_0) \quad (3)$$

where ΔV is the voltage step occurs at the capacitor charging transient, which has

$$\Delta V = i_{arm}(t_0)ESR. \quad (4)$$

This equation reveals the possibility to estimate the ESR with the capacitor charging transient voltage ΔV and the corresponding arm current. However, capturing the transient voltage ΔV has two challenges: 1) extraction of the transient voltage step from the capacitor voltage, with both information of the location and the amplitude; 2) the voltage step caused by the ESR is too small to be captured by the voltage sensors in MMC. To address them, the solutions are given in Sections III and IV.

III. PROPOSED WAVELET-BASED CONDITION MONITORING METHOD

This section proposes to use the DWT to extract the voltage step from the capacitor voltage. An essential challenge of the DWT is the wavelet selection. Based on the established analysis

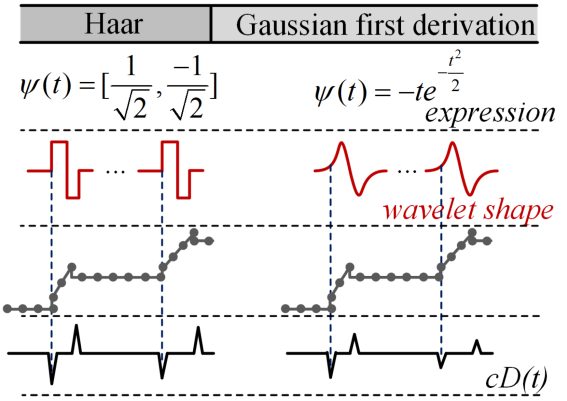


Fig. 4. DWT with the Haar wavelet and Gaussian's first derivation wavelet.

in Section II that the charging transient voltage is a step function, this article selects to use Haar wavelet instead of the conventional Gaussian wavelet [24]. The Haar wavelet is similar to the step voltage at the capacitor charging moment, which is better to extract the step information here and easy to apply in digital processors. Moreover, the reduced complexity alleviates the computations.

The DWT uses a stretched wavelet to calculate the coefficients by shifting the wavelet along the time axis. The obtained wavelet coefficients contain the location and the amplitude information of the transient signals. The location information is given by the wavelet position, while the amplitude information is reflected by the detail coefficient, which is calculated by

$$cD(\alpha, \tau) = \sum_n v(n)\psi_{\alpha,\tau}(n) \quad (5)$$

where cD is the detail coefficient. α, τ represent the scale and shift factors, respectively. $v(n)$ is the input capacitor voltage and n is a positive even integer that indicates the length of it. ψ is the wavelet function.

The wavelet selection is important for the detail coefficient calculation. The similarity between the original signal and the wavelet is one of the criteria in wavelet selection. According to the analysis in Section II, the capacitor charging transient voltage is a step signal, which is similar with the Haar mother wavelet. Therefore, we choose the one-layer Haar wavelet to decompose the capacitor voltage. The comparison of the DWT with Haar wavelet and conventional Gaussian's first derivation wavelet is shown in Fig. 4. Although the location and amplitude information of the transient voltage step can be extracted by both two wavelets, the Haar wavelet used in this article holds two advantages: 1) the Haar wavelet is a kind of discrete wavelet, which fits better for decomposing the practical sampled discrete voltage; 2) the Haar wavelet has a simple expression which alleviates the computation.

With the selected Haar wavelet, the DWT transforms the original signal $v(n)$ to two coefficients of half of its length. The one-layer Haar wavelet used to calculate the detail coefficients

is expressed by

$$\begin{aligned}\psi_{1,1} &= \left(\frac{1}{\sqrt{2}}, \frac{-1}{\sqrt{2}}, 0, 0, \dots, 0 \right) \\ \psi_{1,2} &= \left(0, 0, \frac{1}{\sqrt{2}}, \frac{-1}{\sqrt{2}}, 0, 0, \dots, 0 \right) \\ &\vdots \\ \psi_{1,n/2} &= \left(0, 0, \dots, 0, \frac{1}{\sqrt{2}}, \frac{-1}{\sqrt{2}} \right).\end{aligned}\quad (6)$$

In this way, the detail coefficient of the charging transient voltage is calculated with the Haar wavelet by

$$cD(1, m) = \frac{1}{\sqrt{2}}[v(2m - 1) - v(2m)] \quad (7)$$

where $m = 0, 1, \dots, n/2$. In this way, the relationship between the detail coefficient and the voltage step at the charging transient is

$$cD(1, t_0) = \frac{\Delta V(t_0)}{\sqrt{2}}. \quad (8)$$

Substituting (8) to (4), the ESR can be estimated by

$$\text{ESR} = \left| \frac{\sqrt{2}cD(1, t_0)}{i_{\text{arm}}(t_0)} \right|. \quad (9)$$

From (9), the ESR is only relevant with the capacitor transient information at the charging moment. Although the control strategies and the modulation schemes may change in MMC-based motor drives, the transient information can be extracted as long as the capacitor is charged.

IV. IMPLEMENTATION OF THE PROPOSED CM METHOD

The aforementioned analysis shows a theoretical feasibility to extract the capacitor ESR by the charging transient voltage. This section further demonstrates the implementation, including the minimum hardware design, the potential error analysis, the CM monitoring interval selection and a flowchart.

A. Transient Voltage Measurement Circuit

The small magnitude of the charging transient voltage is challenging to be captured by the voltage sensors of the MMC directly. To extract the transient voltage with minimum hardware, this article utilizes a band-pass filter and the spare channels of the amplifier, as shown in Fig. 5.

The high-amplitude and low-frequency voltage fluctuations are bypassed by a designed band-pass filter to provide a better resolution for the charging transient behavior. Specifically, R_h and C_h form a high-pass filter first. The crossover frequency is set as 2 kHz ($R_h = 2.5 \text{ k}\Omega$ and $C_h = 33 \text{ nF}$) to filter out the low-frequency voltage. Next, R_l and C_l form a low-pass filter against the high-frequency background noise. It should be noted that the crossover frequency of the low-pass filter should be higher than the switching frequency, because the charging transient voltage is highly relevant to the switching behavior.

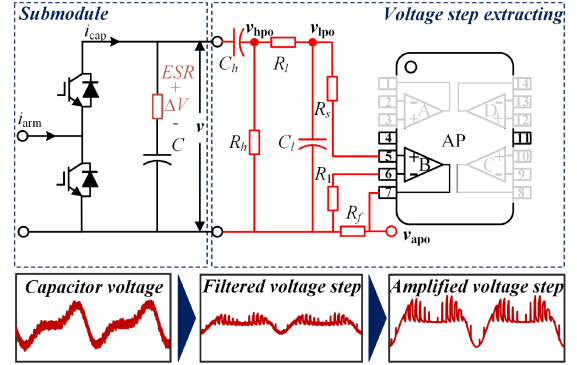


Fig. 5. Minimum hardware design with existing spare amplifier channel.

Therefore, the crossover frequency of 80 kHz ($R_l = 68 \text{ }\Omega$ and $C_l = 33 \text{ nF}$) is selected in this case study.

To fully utilize the measuring range of the voltage sensors or ADs, an amplifier is designed in Fig. 5 with three resistors, i.e., R_1 , R_f , and R_s . The amplifier ICs in MMC SMs usually have spare channels. For instance, a SOIC14 package amplifier (OP4177ARZ) shown in Fig. 5 is one of the typical selections. If the channels A, C, and D are used for capacitor voltage, temperature, and humidity measurement, the spared channel B can be used to capture the charging transient voltage. By this way, the proposed solution only needs several resistors and capacitors to achieve a minimum hardware requirement. In this case, a gain of the amplifier is set as 5 with $R_f = 4 \text{ k}\Omega$ and $R_1 = 1 \text{ k}\Omega$. The v_{apo} is the output of the amplifier.

B. Sampling Frequency Selection

The above analysis is based on the assumption that the sampling instant is synchronized with the voltage step, which rarely happens in a practical system. Therefore, the sampling error caused by unsynchronized sampling instant is analyzed in detail, as shown in Fig. 6. Assuming the first sampling instant is t_0 and the second sampling instant is t_1 , the sampled error is analyzed under three different situations.

Fig. 6(a) shows the situation where the transient voltage step is included in the two sampling instants and the voltage step happens immediately after the first sampling instant. The blue curve represents the ideal sampled voltage with infinite high sampling frequency, while the red curve represents the sampled voltage with a low sampling frequency. Therefore, the ΔV_0 and ΔV are regarded as the ideally and the practically sampled voltage step. The ΔV can be expressed as

$$\Delta V = \Delta V_0 + \Delta v_{\text{cap}} \quad (10)$$

where Δv_{cap} is the additional voltage step caused by the delayed sampling period Δt . As the transient analysis in Section II, Δv_{cap} is dominated by capacitance, which thus has an expression of

$$\Delta v_{\text{cap}} = \frac{1}{C} \int i_{\text{cap}}(t) dt = \frac{1}{C} i_{\text{arm}}(t_0) \Delta t \quad (11)$$

where the charging current $i_{\text{cap}}(t)$ during Δt is considered as a constant and equals to the instantaneous value $i_{\text{arm}}(t_0)$.

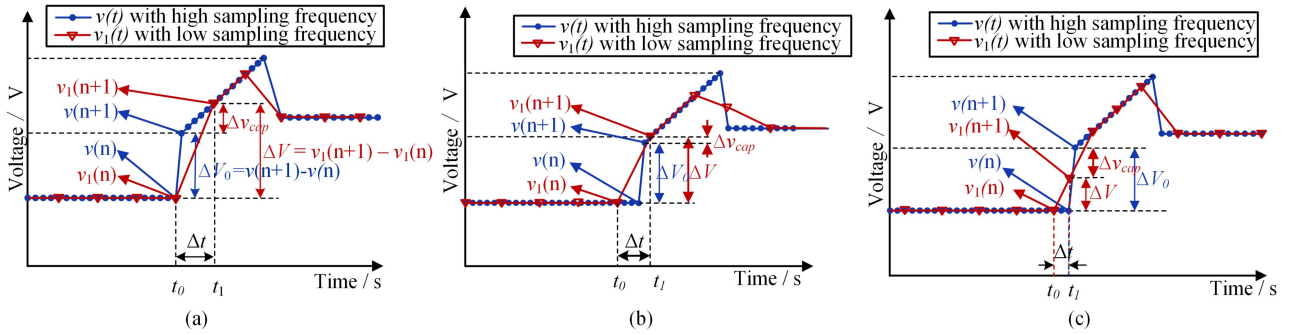


Fig. 6. Charging transient voltage sampling error with low sampling frequency.

Therefore, the practically ESR is overestimated as

$$\text{ESR} = \frac{\Delta V + \Delta v_{\text{cap}}}{i_{\text{arm}}(t_0)} = \text{ESR}_0 + \frac{1}{C} \Delta t. \quad (12)$$

where ESR_0 denotes the initial ESR. The second item in (12) represents the estimation error caused by the delayed sampling. The estimation error σ is defined as

$$\sigma = \frac{\text{ESR} - \text{ESR}_0}{\text{ESR}_0} = \frac{\Delta t}{C \cdot \text{ESR}_0}. \quad (13)$$

The minimum sampling frequency can be preset with a given maximum error according to (13). However, the practical sampling frequency must be higher than the theoretical value considering the additional noise, which is expressed by

$$f_{\text{sample}} > \frac{1}{\sigma \cdot C \cdot \text{ESR}_0}. \quad (14)$$

The estimation error would change when a capacitor is degraded. In a practical degraded capacitor, the capacitance would decrease simultaneously with the increase of the ESR. The end of life (EOL) for an Al-cap is 80% capacitance decrease and two times increase of the ESR. Therefore, the variation of estimation error is discussed with two worst situations: 1) only capacitance changes and 2) only ESR changes. When only the capacitance decreases, the estimation error would be 1.25 times than the initial one, while the error would be 0.5 times than the initial one when only the ESR increases. Therefore, the estimation error would vary 0.5~1.25 times of the initial one during the degradation.

Fig. 6(b) shows the situation where the transient voltage step is included in the two sampling instants and the voltage step happens after the first sampling instant. This situation is similar but better than the aforementioned one because capacitor voltage before the first sampling instant is a constant, therefore, the additional voltage step caused by the delayed sampling period is smaller.

Fig. 6(c) shows the situation where the transient voltage step rising process is sampled by the second sampling instant. In this situation, the estimated ESR would be lower than the real value. The estimation results in this situation are considered as outliers.

Accordingly, the estimated ESR would fluctuate around the real value due to the unsynchronized sampling instants. Therefore, further data analysis methods could be employed to improve the accuracy according to the data distribution characteristics.

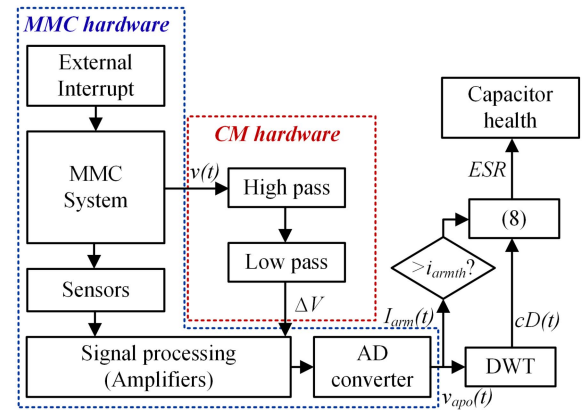


Fig. 7. Flowchart of proposed CM method.

C. Condition Monitoring Interval Selection

The arm current also contributes to additional errors to the estimated ESR according to (9). Specifically, a small drift ε would be introduced to the arm current due to the unsynchronized sampling. The drift is relevant with the current change rate and the unsynchronized time t_ε , which is expressed by

$$\varepsilon = i'_{\text{arm}}(t) \cdot t_\varepsilon = \omega A \cdot \cos(\omega t) \cdot t_\varepsilon \quad (15)$$

where ω is the MMC ac-side line frequency and A is the amplitude of the arm current. $i'_{\text{arm}}(t)$ is the current change rate and equals to the derivation of the arm current. The current change rate is close to 0 when the arm current is measured around its maximum value [$t = \pi/2 \pm 2k\pi$ ($k = 0, 1, 2, \dots$)]. Therefore, the estimation error caused by the small drift can be eliminated by utilizing a preset threshold i_{armth} to extract the maximum arm current. It should be noted that for variable-load condition motor drive-based MMC systems, the threshold should be set according to the current change rate due to the variable current amplitude.

D. Proposed CM Method Flowchart

A flowchart shown in Fig. 7 illustrates the implementation of the proposed method. The dashed blue box shows the existed hardware in a practical MMC system, while the dashed red box shows the additional hardware introduced by the proposed CM method. The transient voltage is extracted by the band-pass filter and enhanced by the amplifier. Meanwhile, the measured arm

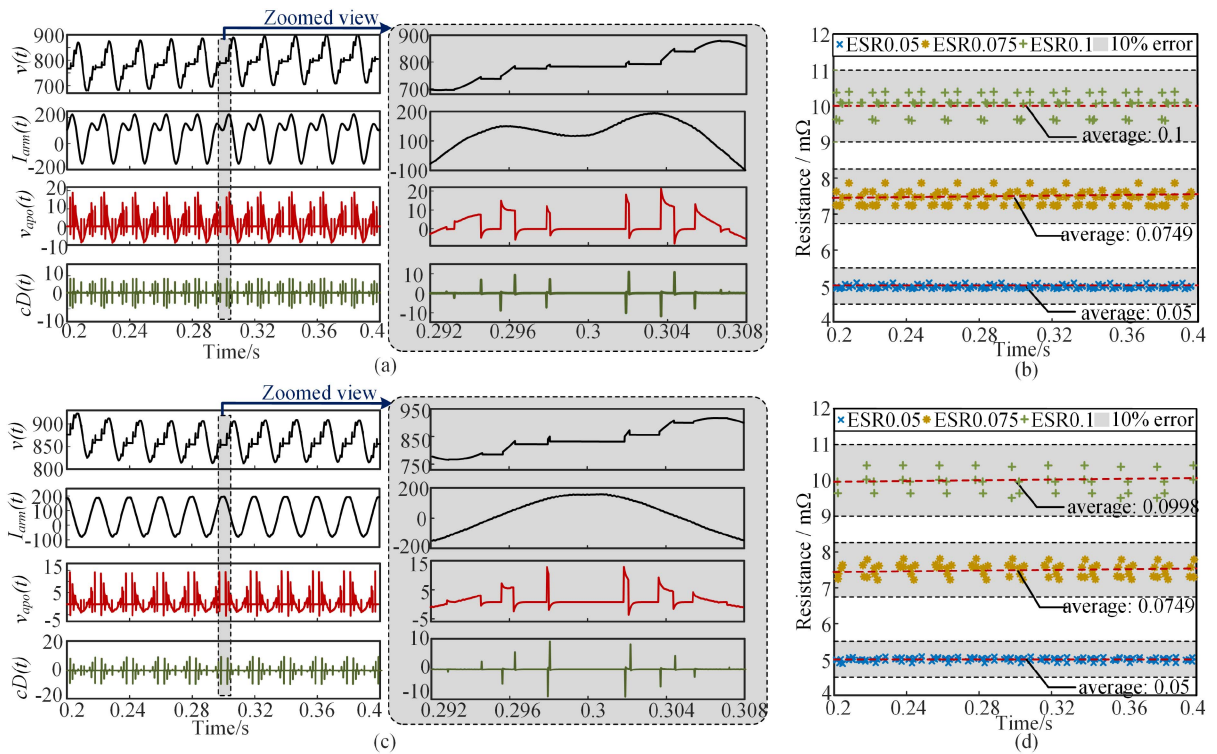


Fig. 8. Extracted signals and ESR estimation results with PSC modulation in the simulation. (a) Without circulating current suppressing control and (b) the corresponding estimated ESR. (c) With circulating current suppressing control and (d) the corresponding estimated.

TABLE II
SIMULATION AND DOWN-SCALED EXPERIMENT PARAMETERS CONFIGURATION

Parameter	Symbols	Simulation	Experiment
		(Full-scale)	(Down-scale)
		Value	Value
Rated power	P	1.2 MW	1.4 kW
Power factor	$\cos\varphi$	0.8	0.8
Phase voltage	$v_j(j=a, b, c)$	4000 V	80 V
dc-bus voltage	V_{dc}	8000 V	200 V
Number of SM per arm	N	10	4
SM capacitance	C_{SM}	2 mF	0.8 mF
Arm inductance	L_{arm}	1 mH	1 mH
carrier frequency of PSC	f_c	500 Hz	1.5 kHz
sampling frequency	f_s	100 kHz	25 kHz

current is compared with the preset threshold i_{armth} to ensure the capacitor is monitored around its maximum value. Then, the ESR is estimated combined with the arm current and the DWT results.

V. SIMULATION VERIFICATION

A three-phase MMC simulation model is established in PLECS to validate the proposed method's robustness to different modulation schemes and control strategies. The parameter of the full-scale simulation model is shown in Table II. The ESR are set as 50 mΩ, 75 mΩ, and 100 mΩ to represent different degradation levels of the capacitor. The influence of system noise on the proposed method is also studied.

A. Effect of Circulating Current Suppressing Control

The effect of circulating current suppressing control strategy is analyzed both in NLM and PSC. The simulation results are shown in Figs. 8 and 9, respectively. The subfigures (a) and (c) show the extracted voltage step and the corresponding detail coefficient without and with the circulating current suppressing control. From the results, the charging transient voltage can be extracted regardless of whether the circulating current suppressing control is activated or not. The DWT further extracts the voltage step from the signal, the location and amplitude information is then obtained by the detail coefficient. According to (13), if the maximum allowable error is set to be 10%, then the minimum sampling frequency should be 100 kHz. The ESR estimation results are shown in (b) and (d), the individual ESR estimation error is limited within 10%. What is more, since the estimated results are evenly distributed, the averaging method is chosen to do the further data analysis according to the aforementioned analysis. The maximum error when taking the average value as the final result is near 0.00% under PSC and 3.5% under NLM.

B. Effect of Different Modulation Schemes

The effect of modulation scheme on the proposed CM method can be analyzed by comparing the results of Fig. 8 with Fig. 9. Different modulation schemes do affect the capacitor's steady-state voltage, where the prior arts are difficult to adapt to the largely varied capacitor behavior. However, the ESR estimation results in (b) and (d) show that the proposed CM method has a

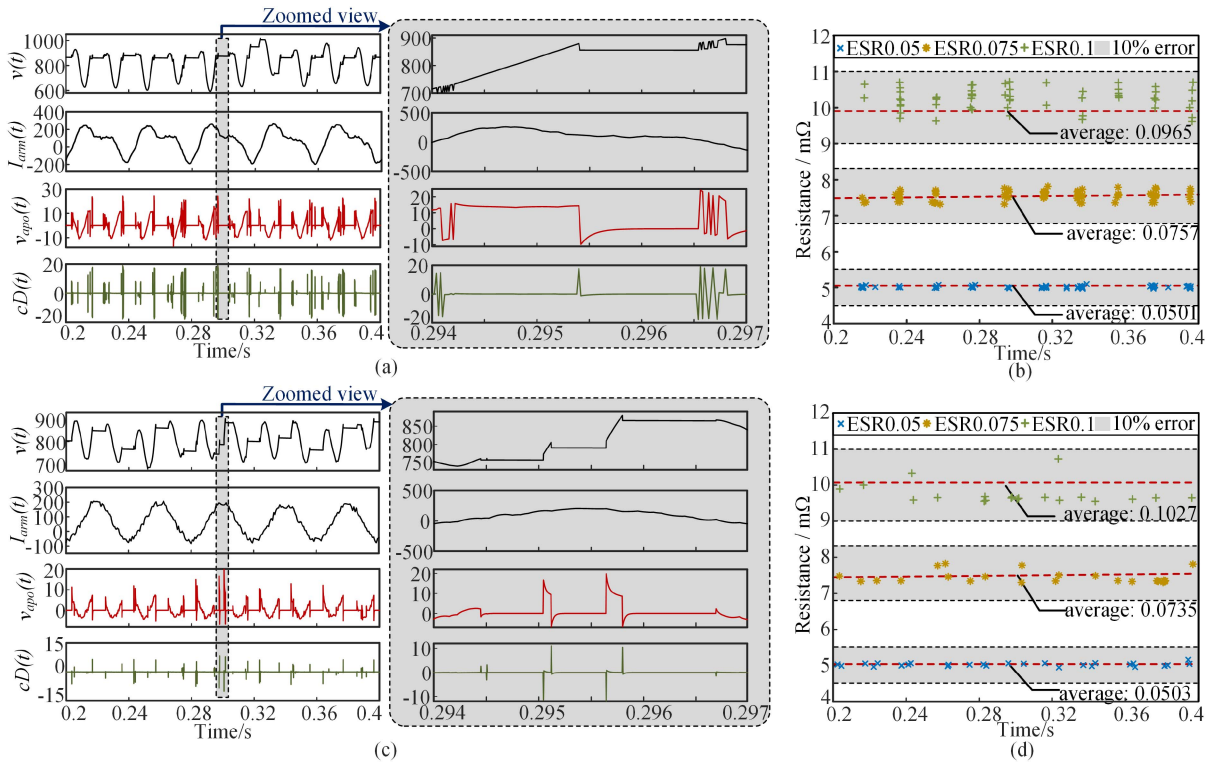


Fig. 9. Extracted signals and ESR estimation results with NLM modulation in the simulation. (a) Without circulating current suppressing control and (b) the corresponding estimated ESR. (c) With circulating current suppressing control and (d) the corresponding estimated.

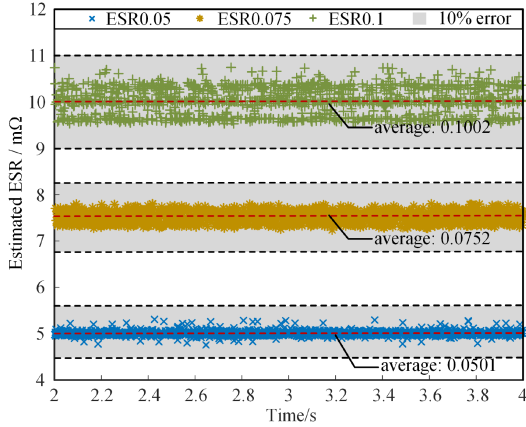


Fig. 10. ESR estimation under NLM in longer timescale.

good robustness to different modulation schemes. The maximum error when taking the average value as the final result is 0.13% under PSC and 2.7% under NLM.

The above ESR estimation results show that the estimation error under NLM is larger than the PSC, which is caused by the different data size in the average value calculation. The switching frequency in NLM is much lower than the PSC, therefore, the charging transients are less in NLM during the same time. The estimation error can be reduced by expanding the estimation time. Fig. 10 shows the estimation results under the NLM scheme in 2 s, which takes the without circulating

current control strategy as an example. The results show that the estimation error can be reduced to 0.2% with longer timescale.

C. Effect of System Noises and Switching Frequency

The ideal charging transient voltage in the simulation proves the feasibility of the proposed method. However, the system noise in a practical system would unavoidably affect the charging transient. To investigate noise's effect, noise with different levels [signal-to-noise ratio (SNR) = no noise, 40, 30, and 20 dB] are added into the original simulated voltage and current signals. The CM results distribution is shown in Fig. 11. From the results, the standard deviation (std) of the CM results increases with the increased noises level. However, the average value of the results always keep close to the real ESR. Therefore, taking the average value as the final result could improves the ESR estimation accuracy.

To investigate the influence of switching frequency, the proposed method is verified with different carrier frequency. The test condition is with PSC modulation scheme, without circulating current suppressing control, and the ESR value is 0.05Ω . The ESR estimation results (average value) are shown in Table III. The results show that the ESR is estimated precisely under different switching frequency.

VI. EXPERIMENTAL VERIFICATION

A three-phase down-scaled MMC platform is built in a laboratory to verify the proposed method, as shown in Fig. 12.

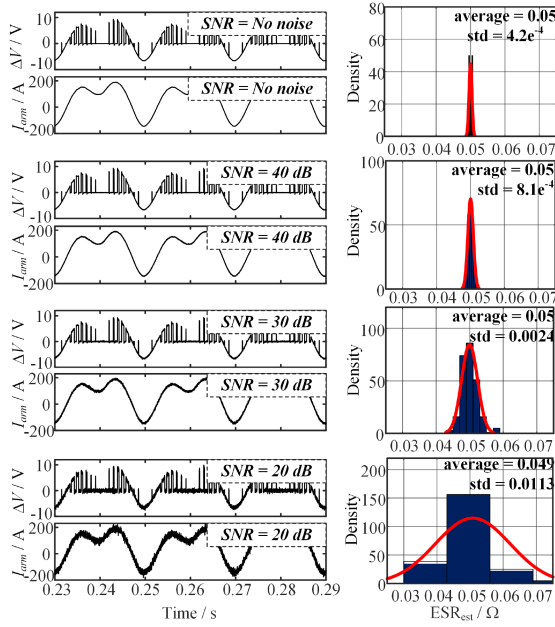


Fig. 11. Noise effect on the proposed CM method (test condition: PSC, without circulating current suppressing control, ESR = 50 mΩ).

TABLE III
ESR ESTIMATION UNDER DIFFERENT SWITCHING FREQUENCY

f_c	200 Hz	400 Hz	500 Hz	800 Hz	1 kHz
ESR _{est}	0.0499 Ω	0.0500 Ω	0.0500 Ω	0.0500 Ω	0.0501 Ω

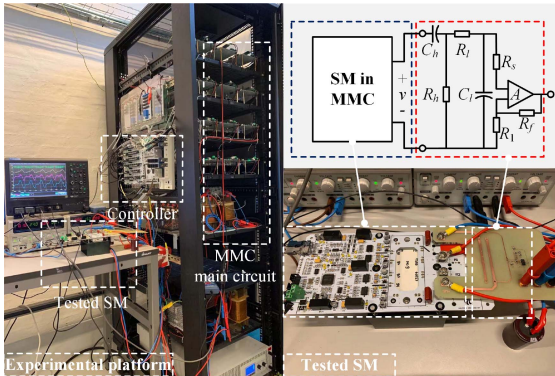


Fig. 12. Three-phase down-scaled MMC platform.

The experimental platform configuration is shown in Table II. As the NLM modulation scheme is usually applied to MMC that the number of SMs is larger than ten. The following experiments are based on the PSC modulation scheme only. The experiments test the effectiveness with and without activating the circulating current suppressing control. To emulate the health status of the capacitor, two groups of capacitor banks are implemented. Group I uses the two parallel identical capacitors, while Group II uses a capacitor only. Compared to Group I, the ESR of Group II increases by 100% which typically regards reaching the one of the end-of-life criteria of Al-Caps.

A. Without Circulating Current Suppressing Control

The experiment results with the circulation current suppressing control are shown in Fig. 13(a) and (b). It shows that the voltage step can be extracted and amplified with the designed hardware in each charging transient, which is v_{apo} . Fig. 13(c) shows the ESR estimation results with v_{apo} , the results fluctuate in a certain range due to the effects of temperature, frequency, noise, etc. To avoid the effect of operation conditions and individual difference, we use two repeated tests under three different load conditions (load resistor R_L = 12.4 Ω, 8.7 Ω, and 4.6 Ω) to show the results distribution. The red central mark indicates the median value, the bottom and top edges of the box indicate the 25th and 75th percentiles, respectively. The outliers are plotted individually using the red “+” marker symbol. It is clear that the noises would lead to many outliers in the estimated ESR, which results in the unevenly distributed results. Therefore, the median value is chosen as the further data analysis method. The median values of the estimated ESR are shown in the table, which are approximately equal in each test. It can be inferred that the ESR estimation is independent of the operation conditions of the converter. Moreover, the average median value of group II is approximately as that of group I, which means the capacitor is degraded.

B. With Circulating Current Suppressing Control

The experimental results without circulating current suppressing control are shown in Fig. 14, where the ESR estimation results are shown in Fig. 14(c). Compared with the results with circulating current suppressing control, the median values of the estimated ESR are not influenced by the control strategy. In addition, the median value of group II is approximately twice of the group I's as expected. Therefore, the robustness to different control strategies of the proposed CM method is verified.

With the experimental results with and without circulating current suppressing control, the degraded capacitor is identified in both situations. Although it is not experimentally proved with the NLM scheme due to the power limit in laboratory, the lower switching frequency of the NLM would make the proposed method easier to be applied. Therefore, the feasibility of the proposed CM method is proved.

The proposed method aims to improve the robustness of previous CM methods to different system control strategies and modulation schemes. However, it still has limitations in practical applications: 1) metallized polypropylene film (MPPF) capacitors are usually employed in high power MMC applications for higher voltage capability. In such cases, the ESR is hard to be detected due to significantly lower values than that of Al-caps. Therefore, the proposed CM method is only applicable in low-to-medium MMC applications (microgrid, motor drive, etc.). 2) Although simple and economic, the minimum hardware design is still invasive to existed MMC projects. However, it can still provide possibility for upcoming MMC projects to monitor capacitor health status.

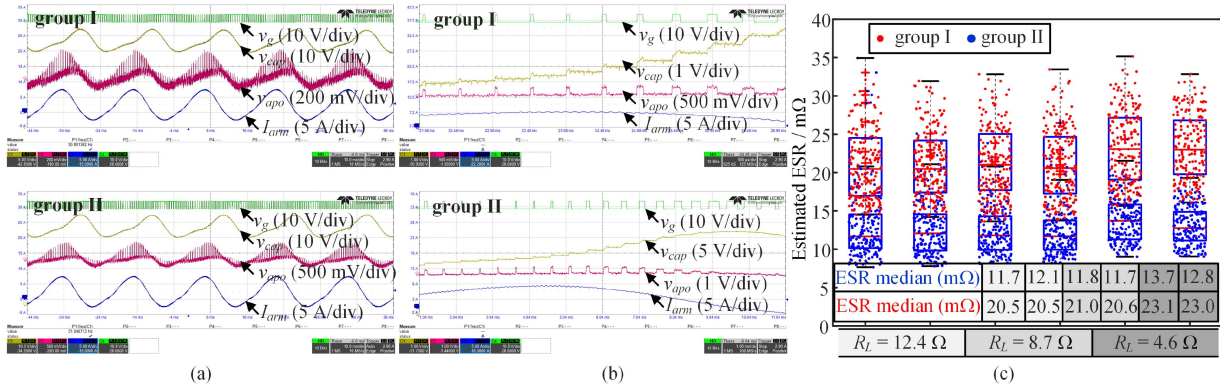


Fig. 13. Experimental results with circulating current suppressing control. (a) Measured signals of group I and II. (b) Zoomed view. (c) ESR estimation results.

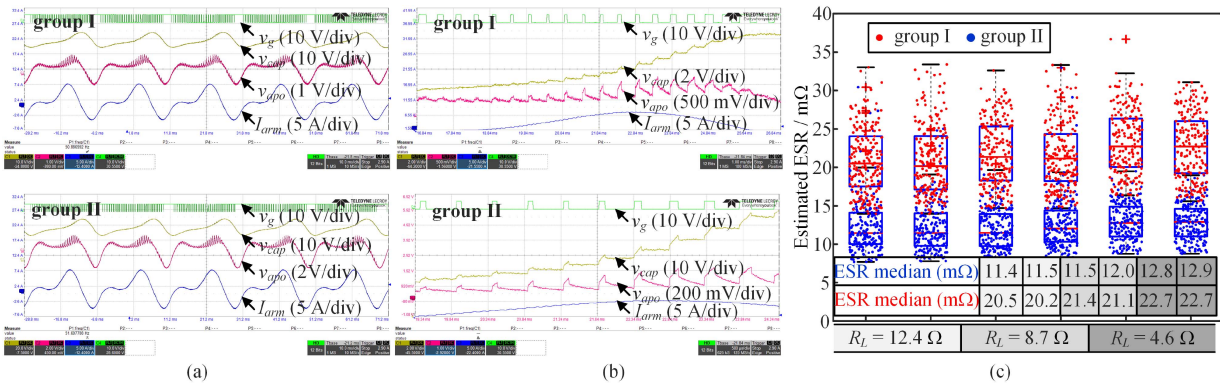


Fig. 14. Experimental results without circulating current suppressing control. (a) Measured signals of group I and II. (b) Zoomed view. (c) ESR estimation results.

VII. CONCLUSION

Previous CM methods for capacitors in MMC are suffering from the effect of varied control strategies and modulation schemes. This article provides a novel CM method by estimating the ESR with the capacitor's charging transient voltage. Based on a 1.2-MW MMC simulation model with different control strategies and modulation schemes, the proposed CM method's robustness is verified. The ESR estimation error with different control strategies and modulation schemes is limited within 10%, and the maximum error is further reduced to 3.5% by using the medium value as the final result. Moreover, the proposed method is further designed considering the practical implementation, including the minimum hardware design, the potential error and noise's effect. Finally, the feasibility of the proposed method is proved in a down-scaled MMC platform.

REFERENCES

- [1] B. Wu, *High-Power Converters and AC Drives*. New York, NY, USA: Wiley, 2017.
- [2] S. Zhou, B. Li, M. Guan, X. Zhang, Z. Xu, and D. Xu, "Capacitance reduction of the hybrid modular multilevel converter by decreasing average capacitor voltage in variable-speed drives," *IEEE Trans. Power Electron.*, vol. 34, no. 2, pp. 1580–1594, Feb. 2019.
- [3] A. Edpuganti and A. K. Rathore, "Optimal pulsewidth modulation for common-mode voltage elimination scheme of medium-voltage modular multilevel converter-fed open-end stator winding induction motor drives," *IEEE Trans. Ind. Electron.*, vol. 64, no. 1, pp. 848–856, Jan. 2017.
- [4] S. Du, B. Wu, and N. Zargari, "A control strategy for star-channel modular multilevel converter in variable-speed motor drive application," *IEEE Trans. Ind. Electron.*, vol. 66, no. 7, pp. 5094–5101, Jul. 2019.
- [5] D. D. Simone, P. Tricoli, S. D'Arco, and L. Piegari, "Windowed PWM: A configurable modulation scheme for modular multilevel converter-based traction drives," *IEEE Trans. Power Electron.*, vol. 35, no. 9, pp. 9727–9736, Sep. 2020.
- [6] H. Soliman, H. Wang, and F. Blaabjerg, "A review of the condition monitoring of capacitors in power electronic converters," *IEEE Trans. Ind. Appl.*, vol. 52, no. 6, pp. 4976–4989, Nov. 2016.
- [7] D. Ronanki and S. S. Williamson, "Failure prediction of submodule capacitors in modular multilevel converter by monitoring the intrinsic capacitor voltage fluctuations," *IEEE Trans. Ind. Electron.*, vol. 67, no. 4, pp. 2585–2594, Apr. 2020.
- [8] Y. J. Jo, T. H. Nguyen, and D. C. Lee, "Condition monitoring of submodule capacitors in modular multilevel converters," in *Proc. IEEE Energy Convers. Congr. Expo.*, 2014, pp. 2121–2126.
- [9] D. Ronanki and S. S. Williamson, "Quasi-online low-frequency impedance monitoring scheme for submodule capacitors in modular multilevel converters," in *Proc. IEEE Appl. Power Electron. Conf.*, 2019, pp. 83–90.
- [10] C. Liu, F. Deng, Q. Yu, Y. Wang, F. Blaabjerg, and X. Cai, "Submodule capacitance monitoring strategy for phase-shifted carrier pulsed-width-modulation-based modular multilevel converters," *IEEE Trans. Ind. Electron.*, vol. 68, no. 9, pp. 8753–8767, Sep. 2021.
- [11] K. Wang, L. Jin, G. Li, Y. Deng, and X. He, "Online capacitance estimation of submodule capacitors for modular multilevel converter with nearest level modulation," *IEEE Trans. Power Electron.*, vol. 35, no. 7, pp. 6678–6681, Jul. 2020.
- [12] Z. Geng, M. Han, and G. Zhou, "Switching signals based condition monitoring for submodule capacitors in modular multilevel converters," *IEEE Trans. Circuits Syst. II Exp. Briefs*, vol. 68, no. 6, pp. 2017–2021, Jun. 2021.
- [13] F. Deng et al., "Capacitor ESR and C monitoring in modular multilevel converters," *IEEE Trans. Power Electron.*, vol. 35, no. 4, pp. 4063–4075, Apr. 2020.

- [14] X. Xin, Y. Yang, K. Ma, and B. He, "Online monitoring for sub-module capacitance in modular multilevel converter with four sampling points of capacitor voltage," in *Proc. IEEE 9th Int. Power Electron. Motion Control Conf.*, 2020, pp. 935–939.
- [15] I. Polanco and D. Dujic, "Condition health monitoring of modular multilevel converter submodule capacitors," *IEEE Trans. Power Electron.*, vol. 37, no. 3, pp. 3544–3554, Mar. 2022.
- [16] O. Abushafa, S. Gadoue, M. Dahidah, and D. Atkinson, "A new scheme for monitoring submodule capacitance in modular multilevel converter," in *Proc. IET Conf. Power Electron. Mach. Drives.*, 2016, pp. 1–6.
- [17] F. Deng, Q. Wang, D. Liu, Y. Wang, M. Cheng, and Z. Chen, "Reference submodule based capacitor monitoring strategy for modular multilevel converters," *IEEE Trans. Power Electron.*, vol. 34, no. 5, pp. 4711–4721, May 2019.
- [18] C. Yin, F. Deng, Q. Yu, Y. Lv, Q. Heng, and Q. Wang, "Capacitor monitoring for full-bridge submodule based modular multilevel converters," in *Proc. Ind. Electron. Conf.*, 2019, pp. 3781–3786.
- [19] N. Yu, S. Shao, X. Wu, J. Zhang, and H. Chen, "Application of tunnel magnetoresistance to health monitoring of modular multilevel converter submodules," in *Proc. IEEE Int. Power Electron. Appl. Conf. Expo.*, 2018, pp. 1–5.
- [20] E. Rodriguez et al., "Capacitor condition monitoring based on an adaptive observer of the low-frequency capacitor voltage ripples for modular multilevel converters," in *Proc. IEEE 4th Int. Future Energy Electron. Conf.*, 2019, pp. 1–6.
- [21] C. Zhang, W. Zhang, S. Ethni, M. Dahidah, V. Pickert, and H. Khalifalla, "Online condition monitoring of sub-module capacitors in MMC enabled by reduced switching frequency sorting scheme," in *Proc. 10th Int. Renewable Energy Congr.*, 2019, pp. 1–6.
- [22] M. Asoodar, M. Nahalparvari, C. Danielsson, R. Soderstrom, and H. P. Nee, "Online health monitoring of DC-link capacitors in modular multilevel converters for FACTS and HVDC applications," *IEEE Trans. Power Electron.*, vol. 36, no. 12, pp. 13489–13503, Dec. 2021.
- [23] Z. Zhao et al., "An online parameters monitoring method for output capacitor of buck converter based on large-signal load transient trajectory analysis," *IEEE J. Emerg. Sel. Top. Power Electron.*, vol. 9, no. 4, pp. 4004–4015, Aug. 2021.
- [24] W. Lu, X. Lu, J. Han, Z. Zhao, and X. Du, "Online estimation of ESR for DC-link capacitor of boost PFC converter using wavelet transform based time–frequency analysis method," *IEEE Trans. Power Electron.*, vol. 35, no. 8, pp. 7755–7764, Aug. 2020.
- [25] M. F. Faisal and A. Mohamed, "Comparing the performance of various mother wavelet functions in detecting actual 3-phase voltage sags," in *Proc. IEEE 2nd Int. Power Energy Conf.*, 2008, pp. 657–661.



Hongjian Xia (Student Member, IEEE) received the B.Sc. degree in electrical engineering from Jilin University, Changchun, China, in 2018. He is currently working toward the Ph.D. degree in electrical engineering with Chongqing University, Chongqing, China.

From 2021 to 2022, he was a Visiting Ph.D. Student with the AAU energy, Aalborg University, Aalborg, Denmark. His research interests include the reliability and control of modular multilevel converters and motor drives.



Yi Zhang (Member, IEEE) received the B.S. and M.S. degrees in electrical engineering from Harbin Institute of Technology, Harbin, China, in 2014 and 2016, respectively, and the Ph.D. degree in electrical engineering from Aalborg University, Aalborg, Denmark, in 2020.

He is currently a DFF International Postdoc affiliated with the Swiss Federal Institute of Technology Lausanne, Vaud, Switzerland. He was a Visiting Scholar with the Georgia Institute of Technology, Atlanta, GA, USA, from November 2018 to February 2019. His research interests include the reliability of power semiconductor devices and power converters, multiphysics modeling, and optimizations.

Dr. Zhang was the recipient of the IEEE Power Electronics Society Ph.D. the Thesis Talk Award in 2020, and the First Place Prize Paper Award from the IEEE TRANSACTIONS ON POWER ELECTRONICS, in 2021.



Minyou Chen (Senior Member, IEEE) received the M.Sc. degree in control theory and engineering from Chongqing University, Chongqing, China, in 1987, and the Ph.D. degree in control engineering from the University of Sheffield, Sheffield, U.K., in 1998.

He is currently a Full Professor with Chongqing University. He has authored or coauthored more than 180 papers. His research interests include intelligent modeling and control, reliability of power modules, microgrid control, state monitoring in power distribution systems.



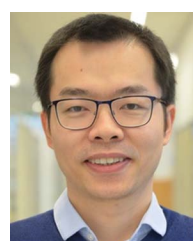
Wei Lai (Member, IEEE) received the M.Sc. degree from the Chongqing University of Technology, Chongqing, China, in 2012, and the joint Ph.D. degree in electrical engineering from the University of Warwick, Coventry, U.K., in 2015, funded by the China Scholarship Council.

He is currently an Associate Professor for Electrical Engineering with the School of Electrical Engineering, Chongqing University, Chongqing, China. His research interests include the reliability of power modules, the application of power electronics for electric power generation, and the development of condition monitoring methods for power electronic converters.



Dan Luo received M.S. degree from the School of Electrical Engineering, Guizhou University, Guizhou, China, in 2016, and the Ph.D. degree in electrical engineering from the School of Electrical Engineering, Chongqing University, Chongqing, China, in 2022.

His research interests include the reliability of power modules.



Huai Wang (Senior Member, IEEE) received the BE degree in electrical engineering from Huazhong University of Science and Technology, Wuhan, China, in 2007 and the Ph.D. degree in power electronics from the City University of Hong Kong, Hong Kong, in 2012.

He is currently a Professor with AAU Energy at Aalborg University, Aalborg, Denmark, where he leads the group of Reliability of Power Electronic Converters (ReliaPEC) and the mission on Digital Transformation and AI. He was a Visiting Scientist with the ETH Zurich, Zurich, Switzerland, from August to September 2014, and with the Massachusetts Institute of Technology, Cambridge, MA, USA, from September to November 2013. He was with the ABB Corporate Research Center, Baden, Switzerland, in 2009. His research interests include the fundamental challenges in modeling and validating power electronic component failure mechanisms and application issues in system-level predictability, condition monitoring, circuit architecture, and robustness design.

Dr. Wang was the recipient of the Richard M. Bass Outstanding Young Power Electronics Engineer Award from the IEEE Power Electronics Society, in 2016, and the 1st Prize Paper Award from IEEE TRANSACTIONS ON POWER ELECTRONICS, in 2021. He serves as an Associate Editor for the *Journal of Emerging and Selected Topics in Power Electronics* and IEEE TRANSACTIONS ON POWER ELECTRONICS.